Magnetic properties of Co-implanted BaTiO₃ perovskite crystal

S. Kazan

Department of Physics, Gebze Institute of Technology, Gebze, 41400 Kocaeli, Turkey
and Institut für Experimentalphysik/Festkörperphysik, Ruhr-Universitaet Bochum, 44780 Bochum, Germany

F. A. Mikailzade

Department of Physics, Gebze Institute of Technology, Gebze, 41400 Kocaeli, Turkey
and Institute of Physics, Azerbaijan Academy of Sciences, 370143 Baku, Azerbaijan

A. G. Şale and M. Maksutoğlu

Department of Physics, Gebze Institute of Technology, Gebze, 41400 Kocaeli, Turkey

M. Acikgoz

Faculty of Arts and Sciences, Bahcesehir University, Besiktas, 34353 Istanbul, Turkey

R. I. Khaibullin, N. I. Khalitov, Ju. I. Gatiiatova, and V. F. Valeev

Kazan Physical-Technical Institute, RAS, Sibirsky Trakt 10/7, 420029 Kazan, Russia

(Received 13 March 2010; revised manuscript received 25 June 2010; published 2 August 2010)

The results of electron magnetic resonance (EMR) and magnetization measurements of Co-implanted barium titanate (BaTiO₃) perovskite crystal are presented. It has been revealed that the implantation with Co on different fluencies of metal concentrations produces a granular composite film in the surface layer of BaTiO₃ substrate, which exhibits remarkable ferromagnetic behavior. EMR measurements revealed spectra originated from iron impurities of BaTiO₃ substrate. Ferromagnetic resonance spectra from Co-implanted surface layer, exhibiting an out-of-plane uniaxial magnetic anisotropy, were also observed. The magnetization measurements performed in various geometries show that the ferromagnetic Co:BaTiO₃ system displays easy-plane magnetic anisotropy. It has been shown that the magnetization and coercivity of ferromagnetic state depends on the fluence of implantation. The observed phenomena are discussed on the basis of strong magnetic dipolar interaction between Co nanoparticles inside the granular composite film formed as a result of implantation.

I. INTRODUCTION

In recent years there has been a continually increasing interest in magnetoelectric (ME) materials due to their attractive physical properties, multifunctionality, wide applications in the fields of sensors, data storage, transducers for magnetic-electric energy conversion, information technology, radioelectronics, optoelectronics, and microwave electronics.[1] In these materials the coupling interaction between ferroelectric and ferromagnetic substances may produce a magnetoelectric effect in which change in magnetization can be induced by an electric field or change in electric polarization can be induced by an applied magnetic field.[2] As it is known from the literature, a strong ME effect could be realized in the composite exhibiting magnetostrictive and piezoelectric effects. It was recently discovered that composite materials and magnetic ferroelectrics exhibit magnetoelectric effects that exceed previously known effects by orders of magnitude[3] with the potential to trigger magnetic or electric phase transitions.

Hence, the fabrication and characterization of new composite structures, especially those based on the intensive incorporation of magnetic nanoparticles into the crystal matrix of ferroelectric perovskite oxides, are of great interest. The magnetic properties of such composites can be controlled on a large scale by varying the average nanoparticle size distribution, packing factor and composition of the magnetic inclusions and surrounding ferroelectric medium.

The search for new and development of the existing technologies of obtaining composite materials with tailor-made structural and magnetic characteristics is currently an important task. Among the different techniques, ion implantation is a very attractive and prospective preparation method, due to easy control of the metal distribution and concentration, the availability of almost arbitrary metal-dielectric compositions, and the ability to surpass the solubility limits constrained by the chemical and thermodynamic equilibrium of the host matrix and metal impurities.[4] Besides, the ion implantation technique is ideally suited for fabrication of thin-film magnetic media and planar devices for magnetosensor electronics.

In this paper the results of investigation of magnetization and electron magnetic resonance[5] (EMR) spectra of Co-implanted BaTiO₃ in a wide temperature range are presented. These results show the promise of magnetic nanocomposites based on ferroelectric perovskites for potential magnetoelectric applications as well as the flexibility of ion implantation as a powerful method for modification of magnetic properties of materials.

II. EXPERIMENTAL METHOD

The $10 \times 10 \times 0.4$ mm³ single-crystalline (100)- or (001)-face oriented plates of cubic (normal) c-BaTiO₃ (supplied by
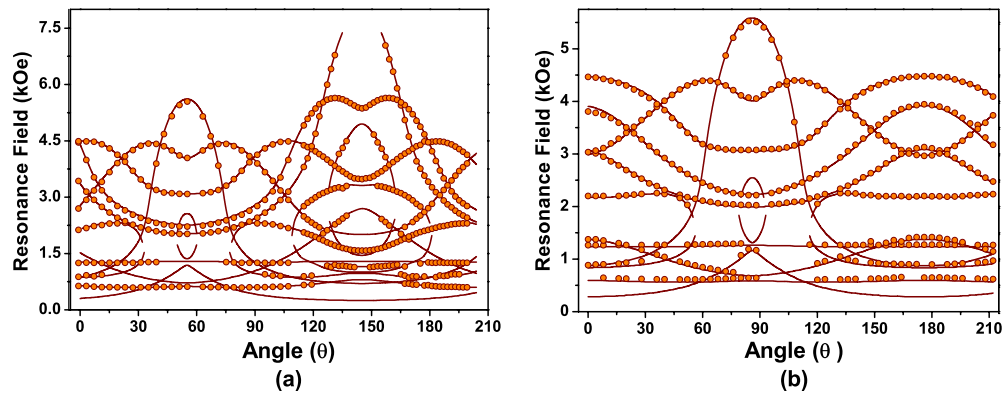
FIG. 1. (Color online) The observed and fitted rotation patterns of the EMR resonance field values of $BaTiO_3$ substrate containing Fe impurities for the rotation of external magnetic field (a) in (001), (b) in (100) crystallographic planes of the sample at room temperature. Solid circles represent the experimental resonance lines. Full curves are calculated using the fitted spin-Hamiltonian parameters.

Crystec GmbH, Berlin, Germany) were implanted with 40 keV Co^+ ions at ion current density of 8 $\mu A/cm^2$ using the ILU-3 ion accelerator (Kazan Physical-Technical Institute of Russian Academy of Science). The sample holder was cooled by flowing water during the implantations to prevent samples from overheating. The implantation fluence varied in the range of $0.5-1.5 \times 10^{17}$ ion/cm^2. After implantation, the samples were cut by a diamond cutter into smaller pieces for the subsequent structural and magnetic studies.

Elemental composition and surface morphology of the implanted samples have been studied using Philips XL30 SFEG scanning electron microscope (SEM). Magnetic-resonance measurements were carried out by using Bruker EMX model X-band (9.8 GHz) spectrometer. A closed-cycle helium cryostat system and Lakeshore 340 model temperature controller were used in the measurements, which allowed to scan the temperature with a rate of about 0.2 K/min and to stabilize the temperature with accuracy better than 0.05 K. The measurements were performed in the temperature range of 10–300 K. The static magnetic field was varied in the range of 0–1600 mT. A goniometer was used to rotate the sample holder which is parallel to the microwave magnetic field and perpendicular to the applied static magnetic field. The measurements were performed in two different, in-plane and out-of-plane, geometries. At the in-plane geometry the sample was attached horizontally at bottom edge of sample holder and the static magnetic field was scanned in the plane of the implanted surface. At the out-of-plane geometry the sample was attached to the flat platform of sample holder whereas the magnetic field of microwave lie in the film plane during measurement and static magnetic field is rotated from the sample plane to the surface normal. The field derivative of microwave power absorption (dP/dH) was recorded as a function of the dc field. To obtain intensities of EMR and ferromagnetic resonance (FMR) signals the double digital integration of the resonance curves were performed using Bruker WINEPR software package (Bruker Bio Spin Corporation, Billerica, MA 01821 USA). The static magnetization measurements made by vibrating-sample magnetometer (VSM) (PPMS, Quantum Design Corp.) for parallel and perpendicular orientations of the applied magnetic field with respect to the implanted surface plane in a wide temperature interval.

Additionally, in the aim of revealing possible magneto-electric coupling in $Co:BaTiO_3$ composite structure, magnetic field dependence of the capacitance of Co-implanted $BaTiO_3$ crystal was measured using Agilent 4287A *LCR* meter.

III. RESULTS AND DISCUSSION

A. Room-temperature EMR studies

The magnetic resonance investigations of Co-implanted $BaTiO_3$ have revealed EMR spectra and FMR spectra, which can be interpreted as an evidence of paramagnetic centers inside the crystal structure, and as the existence of ferromagnetic ordering inside the structure of the implanted samples, respectively. SEM imaging of the surface morphology of the samples implanted at different fluencies revealed the formation of granular surface layer characterized by high-density distribution of Co particles as a result of implantation. The size of the particles was between 5 and 20 nm for the implantation fluency of 1.5×10^{17} ion/cm^2. The FMR spectra [Fig. 4(b)] may originate from the granular composite layer, which consists of ferromagnetic cobalt particles dispersed in the surface layer of ferroelectric $BaTiO_3$ substrate.

On the other hand, the analysis of the EMR spectra of Co-implanted $BaTiO_3$ has revealed an unexpected behavior. It has been established that the EMR lines originate from isolated paramagnetic Fe^{3+} centers located in Ti^{4+} sites. Actually the EMR signals were observed also for the virgin $BaTiO_3$ plates so the substrates were found to contain Fe^{3+} impurities. The rotational EMR patterns for "in-plane" and "out-of-plane" geometries are presented in Fig. 1.

Interpretation of the EMR spectra assumes that the paramagnetic impurity ions are located substitutionally on the titanium (Ti^{4+}) sites due to their ionic radius and are octahedrally coordinated with six-nearest-neighbor oxygen ligands, which gives rise to crystal field with cubic symmetry at Ti^{4+} sites. The analysis of magnetic resonance measurements of both implanted and virgin $BaTiO_3$ substrates suggests that the EMR spectra originate from iron impurities in the virgin $BaTiO_3$ substrate. Note that the EMR spectra from paramagnetic Fe centers in $BaTiO_3$ were observed earlier.[6–10] In most cases, the authors considered the EMR lines as originating

from Fe^{3+} ions located at Ti^{4+} sites, thus pointing to the existence of uniaxial distortions of crystal fields due to Fe^{3+}-V_o vacancies formed due to the charge compensation.[11]

The degeneracy of spin multiplet of the S-state Fe^{3+} ion ($S=5/2$, $L=0$) is removed due to the spin-orbit coupling and crystal field due to the surrounding anion ligands.[12] Using the equivalent Stevens operators, the energy-level splitting of Fe^{3+} ion can be described by the Spin Hamiltonian

$$H = H_Z + H_{ZFS} = \mu_B \vec{B} \vec{\vec{g}} \vec{S} + \sum_{m=0}^{2} B_2^m O_2^m + \sum_{m=0}^{4} B_4^m O_4^m, \quad (1)$$

where $S=5/2$ is the electronic spin and μ_B is Bohr magneton. The first term H_Z accounts for the Zeeman interaction, the second term H_{ZFS} is the zero-field splitting (ZFS) Hamiltonian. The Stevens operators O_4^m are defined according to Abragam and Bleaney[13] for orthorhombic and higher symmetry. Extended Stevens operators $O_k^q (S_x, S_y, S_z)$ for monoclinic and triclinic symmetries were defined in Refs. 14 and 15. For the Fe^{3+} ions in cubic sites with a tetragonal distortion, the ZFS Hamiltonian[10,12] is

$$H_{tetr} = B_2^0 O_2^0 + B_4^0 O_4^0 + B_4^4 O_4^4. \quad (2)$$

Using the spin and ZFS Hamiltonian in Eqs. (1) and (2), the computer simulations of the EMR spectra of Fe^{3+} center in $BaTiO_3$ crystal were performed and the spin Hamiltonian parameters were determined as listed in Tables II and III. As it is seen above, the observed and fitted EMR rotation patterns exhibit small deviation of the ZFS at Fe^{3+} site from the cubic symmetry by the way of tetragonal distortion,[13] which is attributed to the existence of the tetragonal ferroelectric phase in $BaTiO_3$ crystal in the temperature range between 5 ° and 120 °C.[8]

Considering the g factor which is isotropic for the cubic symmetry. Two $(g_\parallel, g_\perp)$ or three (g_x, g_y, g_z) components of g factor exist for tetragonal and orthorhombic symmetries. The anisotropy of g factor can appear as a deviation from the free electron spin g factor. g factor for the paramagnetic Fe^{3+} ions in ferroelectric tetragonal phase of $BaTiO_3$ was mostly determined as isotropic and is very close to the free electron spin value.[10] Due to the small anisotropy, the isotropic g factor for Fe^{+3}:$BaTiO_3$ may be good approximation by considering the computational procedure and experimental errors, (reading of resonance field correctly, tune conditions during measurements, replacement of sample in right geometry). The value of g factor was calculated from the fitting of angular variation in resonance lines at room temperature as 2.0036.

Additionally, the superposition model (SPM) (Refs. 19–24) has been used to calculate the theoretical ZFS parameters for Fe^{3+} ions at the substitutional sites in $BaTiO_3$ crystal to compare with the experimental data. The ZFS parameters for Fe^{+3} ions in $BaTiO_3$ were calculated in several papers.[24–30] A review of the g factors and ZFS parameters for Fe^{3+} ions in $BaTiO_3$ reported by various authors has appeared in Ref. 10. The theoretical calculations of ZFS parameter by using the density of state calculations was performed in Refs. 31 and 32. According to SPM, the ZFS parameters can be expressed as[22–24]

TABLE I. Crystal structure data of $BaTiO_3$ crystal. The reference distance is chosen to be $c_0/2$ (c_0 is the lattice parameter).

	Crystal structure data of $BaTiO_3$			
	R (nm): the distance of the ith ligand		θ (deg)	Reference
Ti site	R_0	0.2018	86.64	33 and 34
	R_1	0.2002		34
	R_2	0.1860		34
	R_3	0.2174		34
	c_0 (nm)	0.40361		35

$$b_k^q = \sum_i \overline{b}_k(R_i) K_k^q(\theta_i, \phi_i), \quad (3)$$

where the coordination factors K_k^q, which were defined in Ref. 23, are functions of the angular positions (angles θ_i and ϕ_i) of the ligands at a given distance R_i from the paramagnetic ion and full listing of K_k^q was provided in Ref. 24. The $K_k^q(\theta_i, \phi_i)$ functions were tabulated in Refs. 20 and 24. For arbitrary symmetry, whereas those required for Fe^{3+} ions in tetragonal symmetry are

$$K_2^0 = \frac{1}{2}(3 \cos^2 \theta - 1),$$

$$K_4^0 = \frac{1}{8}(35 \cos^4 \theta - 30 \cos^2 \theta + 3),$$

$$K_4^4 = \frac{35}{8} \sin^4 \theta \cos 4\phi. \quad (4)$$

The intrinsic parameters $\overline{b}_k(R_i)$ in Eq. (3) obey the power law

$$\overline{b}_k(R_i) = \overline{b}_k(R_0) \left(\frac{R_0}{R_i}\right)^{t_k}, \quad (5)$$

where R_i and R_0 are the distance of the ith ligand and the reference distance, respectively; t_k are the power-law exponents which are adjustable semiempirical parameters like $\overline{b}_k$. R_i is typically different from the corresponding cation-anion distance R_h due to the difference between the radii of host (r_h) and substituted atoms (r_i), and may be approximated by the formula[15]

$$R_i \approx R_h + \frac{1}{2}(r_i - r_h). \quad (6)$$

For Ti-Fe substitution in $BaTiO_3$, r_i is 0.061 nm and r_h is 0.068 nm.[19] Using Eq. (6) and R_h values,[20] we obtain R_i values tabulated in Table I and are inserted in Eq. (5). Finally, considering the "scaled" parameters $b_k^q = f_k B_k^q$, where $f_k=3$ and 60 for $k=2$ and 4, respectively,[5,12–14] SPM provides the following equations for fine-structure spin Hamiltonian parameters at sixfold coordinated Ti^{4+} sites with D_{4h} symmetry[20,22,24]

TABLE II. The second-rank ZFS parameters B_2^0 (in 10^{-4} cm^{-1}) for Fe^{3+} ion at Ti^{4+} site in BaTiO$_3$ crystal calculated using SPM.

	Set (a) (Refs. 16 and 17)	Set (b) (Ref. 16)	Set (c) (Ref. 18)	Experimental (this work)
t_2	8	7	8	
$\overline{b}_2(R_0)$	−4120	−4120	−5400	
B_2^0	416	316	545	336

$$b_2^0 = 3B_2^0 = \overline{b}_2(R_0)\left[2\left(\frac{R_0}{R_1}\right)^{t_2}(3\cos^2\theta - 1)\right.$$
$$\left. + \left(\frac{R_0}{R_2}\right)^{t_2} + \left(\frac{R_0}{R_3}\right)^{t_2}\right],$$

$$b_4^0 = 60B_4^0 = \overline{b}_4(R_0)\left[\frac{1}{2}\left(\frac{R_0}{R_1}\right)^{t_4}(35\cos^4\theta - 30\cos^2\theta + 3)\right.$$
$$\left. + \left(\frac{R_0}{R_2}\right)^{t_4} + \left(\frac{R_0}{R_3}\right)^{t_4}\right],$$

$$b_4^4 = 60B_4^4 = \frac{35}{2}\overline{b}_4(R_0)\left(\frac{R_0}{R_1}\right)^{t_4}\sin^4\theta \qquad (7)$$

Considering the ligand contributions of six O^{2-} nearest neighbors to the Fe^{3+} paramagnetic ion at Ti^{4+} site and using Eq. (3) the second- and fourth-rank ZFS parameters have been calculated for Fe^{3+} ion in BaTiO$_3$ using two different sets of model parameter and the structural data in Table I are listed together with the experimental data in Tables II and III, respectively. Our SPM analysis of ZFS parameters indicates that satisfactory agreement can be achieved between the ZFS parameters measured by EMR and those predicted by SPM for Fe^{3+}:BaTiO$_3$.

B. Low-temperature magnetic resonance studies

The low-temperature magnetic resonance spectra of Co-implanted BaTiO$_3$ substrates with Fe impurities are shown in Fig. 2. The measurements were performed in the (001) and (100) planes of the sample in the temperature range between 10 and 300 K. Figure 2 reveals that the low-temperature spectra contain both EMR and FMR lines, which vary with temperature. The narrow multiple resonance lines which have a linewidth of 20 Oe as shown in Fig. 2 is due to the

paramagnetic Fe^{3+} ions and broad resonance signal at about 2 kOe is attributed to the FMR resonance line due to the ferromagnetic granular film consisted of Co nanoparticles. The linewidth of this broad FMR resonance field at perpendicular geometry [the magnetic field component of microwave and external static magnetic field lie in (001) plane of the sample] is approximately 1 kOe. The temperature dependence of FMR line can be interpreted taking into account the temperature dependence of the effective magnetization, which is discussed in subsequent sections. The EMR resonance lines exhibit considerable changes at temperature about 276 and 176 K, which may be attributed to the structural phase transitions in BaTiO$_3$.[26,27,36–38] The angular variations in the EMR spectra obtained by rotating the sample in the in-plane [with the static magnetic field rotated in (001) plane of crystal] and out-of-plane geometries [the static magnetic field rotated in the (100) or (010) plane] as well as the experimental and simulated rotation patterns of the resonance fields at the orthorhombic phase temperatures are presented in Fig. 3. Almost the same result has been obtained in the second out-of-plane geometry, which is perpendicular to the first one. Figure 3 shows two groups of anisotropic EMR lines in the orthorhombic phase of BaTiO$_3$. The former group consists of two lines arranged symmetrically around the field value corresponding to the *g* value about of 2 while the other group consists of more anisotropic and less intensive resonance lines.

Observation of EMR signal at lower symmetric ferroelectric phases may be difficult due to the formation of complex domain structure.[26] At tetragonal phase the spontaneous polarization occurs along any one of [100] crystallographic direction. Then the axis of distortion in one plane is unique and perpendicular to each other. Then the EMR spectrum consists of resonance line of Fe^{3+} at axial symmetry which is interpreted above using the superposition model. When the crystal transforms from tetragonal to orthorhombic phase, the *c* domains (i.e., domains which have their polarization

TABLE III. The fourth-order ZFS parameters B_4^q (in 10^{-4} cm^{-1}) for Fe^{3+} in BaTiO$_3$ calculated using SPM.

	Set (a) (Refs. 16 and 17)	Set (b) (Ref. 16)	Experimental (this work)
t_4	16	14	
$\overline{b}_4(R_0)$	9.9	29.1	
B_4^0	0.7	1.92	0.793
B_4^4	2.47	7.25	3.5
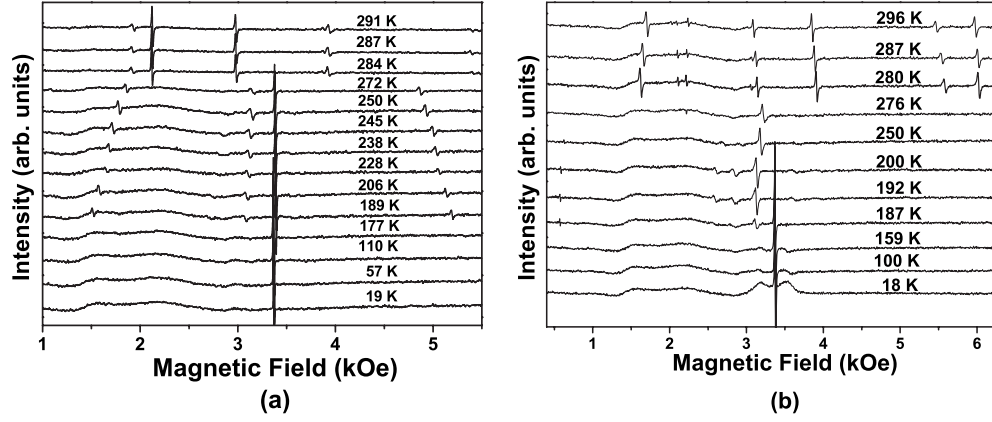
FIG. 2. Temperature dependence of the EMR spectra of $BaTiO_3$ substrate containing Fe impurities measured in the (a) (001) plane (b) (100) plane.

parallel to the c axis) are split into domains which are polarized along any one of six equivalents [110] direction. In this case the observed EMR spectrum will now be obscured by the overlapping of many lines originating from various ion sites with different polar axes.[26] For theoretical interpretation of the observed rotational patterns of EMR spectra, two magnetically equivalent paramagnetic centers with different polar axes aligned in two perpendicular layers were taken into account for Fe^{3+} ions located at oxygen octahedron was used.[10,13] The angular dependences of the resonance fields in the both of the measurements at (001) plane and (100) plane of samples are shown in Fig. 3. The fitted spin Hamiltonian parameters, by means of Eq. (2), are $|B_4^4| = 5.14 \times 10^{-4}$ cm^{-1}, $|B_4^0| = 1.028 \times 10^{-4}$ cm^{-1}, $|B_2^0| = 243 \times 10^{-4}$ cm^{-1}, and $g = 2.0036$. The sign of B_2^0 was found to be opposite to that of B_4^4 as in the case of tetragonal phase. During the phase transformation the magnitude of B_4^4 does not change more but the magnitude of B_2^0 is decreased.

C. Ferromagnetic resonance studies

In magnetic resonance measurements of Co-implanted $BaTiO_3$ sample we observed paramagnetic signals which are attributed to the Fe impurities in sample. In addition to paramagnetic signal, we observed broad resonance signal at high-field region of spectrum as seen in Fig. 4(b). When the external magnetic field is parallel to the implanted surface of $BaTiO_3$ crystal (parallel geometry), the observed signal intensity is very low according to the paramagnetic signals. During the rotation of sample as the magnetic field turns from the implanted surface toward to the normal of implanted surface (perpendicular geometry), the broad signal moved to the high-field region of spectrum and the intensity of this signal increased. The linewidth of this signal is approximately 350 Oe at perpendicular geometry. This broad resonance line is attributed to the ferromagnetic resonance signal due to the granular film composed of Co nanoparticles on the surface. Due to the size and shape distribution of particles on the surface give very broad and low-intensity FMR signal at parallel geometry. We did not observe anisotropic behavior of this FMR line at in-plane geometry. We note that the observed FMR line dependence on the sample orientation is similar to that observed in the FMR of granular magnetic films.[39] In latter case the resonance signal is due the collective motion of particles magnetic moments, i.e., may be described approximately by the macroscopic magnetization of the granular layer as the whole system.

Hence it is possible to analyze the FMR signal as coming from a thin magnetic film with some effective values of the magnetization and g factor. Then, the magnetic free-energy density E for the granular film at arbitrary orientation may be used continuous film[40–42]

$$E = E_z + E_b,$$

$$E_z = -M_0 H[\sin\theta \sin\theta_H \cos(\varphi_H - \varphi) + \cos\theta\cos\theta_H],$$

$$E_b = K_{eff}\cos^2\theta, \quad K_{eff} = (2\pi M_0 - K_\perp), \tag{8}$$

where E_z and E_b are the Zeeman and the bulk (overall) anisotropy energy terms, respectively. M_0 is the saturation magnetization, φ (respectively, φ_H) is the in-plane angle between the magnetization M (respectively, external magnetic field H) and x axis while θ (respectively, θ_H) is the out-of-plane angle between the magnetization M (respectively, external magnetic field H) and z axis as shown in Fig. 4. $K_\perp$ is the perpendicular anisotropy constant. K_{eff} is the effective bulk (shape-demagnetizing) anisotropy constant related to M_{eff} as $4\pi M_{eff} = 2K_{eff}/M_0$. For the resonance condition we used the classical ferromagnetic resonance equation[43]

$$\frac{\omega_o}{\gamma} = \frac{1}{M\sin\theta}(E_{\theta\theta}E_{\varphi\varphi} - E_{\theta\varphi}^2)^{1/2}. \tag{9}$$

$E_{\theta\theta}$ and $E_{\varphi\varphi}$ are second derivatives of E with respect to θ and φ, respectively. Using Eqs. (8) and (9) we obtain the following resonance equation for the out-of-plane geometry:[44]

$$\left(\frac{w}{\gamma}\right)^2 = [H\cos(\theta_H - \theta) - 4\pi M_{eff}\cos^2\theta]$$

$$\times [H\cos(\theta_H - \theta) - 4\pi M_{eff}\cos 2\theta] \tag{10}$$

with
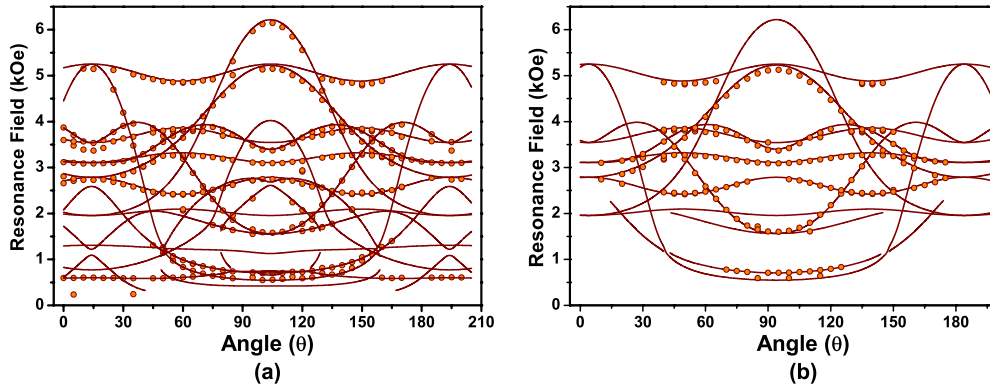
FIG. 3. (Color online) (a) Angular dependence of resonance field at 215 K for the rotation of magnetic field in (100) plane of single-crystalline BaTiO$_3$. (b) Angular dependence of resonance field at 220 K for the rotation of magnetic field in (001) plane of single-crystalline BaTiO$_3$. The solid circles show the experimental position of each resonance line in EMR spectra. The solid lines show the simulation of angular behaviors of the resonance lines.

$$H \sin(\theta - \theta_H) = 2\pi M_{eff} \sin(4\theta). \qquad (11)$$

The value of the *g* factor and effective magnetization were calculated from the variation in resonance field with the rotation angle of sample in the out-of-plane geometry as 2.1 Oe and 630 Oe, respectively. The observed peculiarities of the ferromagnetic behavior of Co-implanted BaTiO$_3$ may be attributed to the dipole-dipole interaction of magnetic cobalt nanoparticles formed as a result of high-influence implantation. This phenomenon (called magnetic percolation) is discussed details in Refs. 39 and 45. The fact is that when the distance between the magnetic particles becomes comparable with their sizes, the dipole-dipole interaction couples the particle magnetic moments. As a result, the granular phase behaves as a ferromagnetic continuum with respect to the dipolar forces even without direct contact between the particles. The mechanism of such dipole-dipole interaction is discussed also in Ref. 46; the authors considered a semiquantitative model for dipolar field for regular array of closely separated spherical particles in granular magnetic layer. This model predicts the dipolar field exhibiting an anisotropic behavior. Hence, the angular dependence of FMR spectra in such systems is qualitatively similar to that of a magnetic thin film.

D. Magnetization measurements

In order to further investigate the magnetic properties of the Co-implanted BaTiO$_3$ we have performed temperature-dependent magnetization $M(T)$ measurements using a VSM magnetometer in field-cooled (FC) and zero-field-cooled (ZFC) regimes. For ZFC measurements, the samples are cooled in zero field to 10 K and the magnetization is recorded during heating the sample up to 400 K under the magnetic field of 100 Oe applied parallel to the sample surface. For FC measurements the applied field of 100 Oe is kept constant during cooling to 10 K and the magnetization is recorded on heating regime on applying the magnetic field of the same intensity. Figure 5 shows that the FC and ZFC curves diverge substantially from each other below 400 K, above which the coincidence of FC and ZFC curves takes place. So, the peculiarities of FC and ZFC curves reveal the presence of superparamagnetic behavior at the temperatures above $T_b \sim 400$ K, which can be considered as "blocking temperature." So, the FC and ZFC curves show ferromagnetic-like behavior up to high temperatures, and the behavior of the magnetization is typical for magnetic granular systems with wide particle size distribution and strong magnetic interaction between particles.[47]
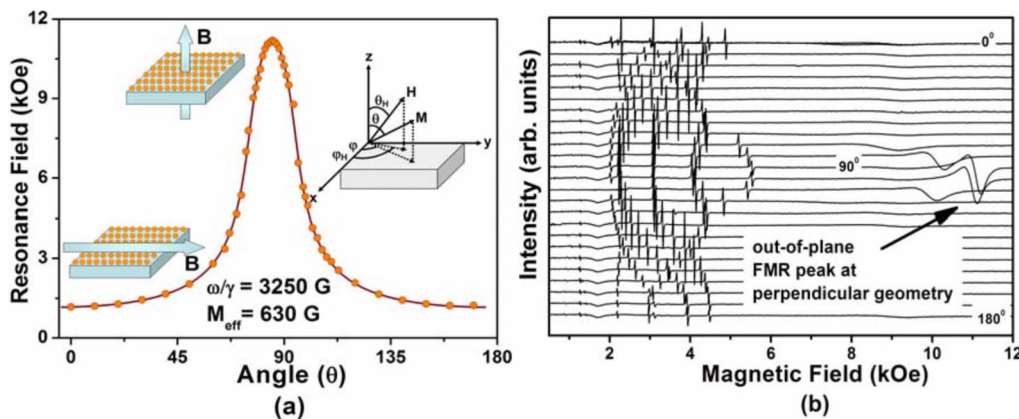
FIG. 4. (Color online) (a) Angular dependence of the FMR resonance field in Co-implanted surface of BaTiO$_3$ in the out-of-plane geometry. The inset figure shows the coordinate system for FMR measurements. (b) The FMR spectra of the Co-implanted surface of BaTiO$_3$ at out-of-plane geometry.
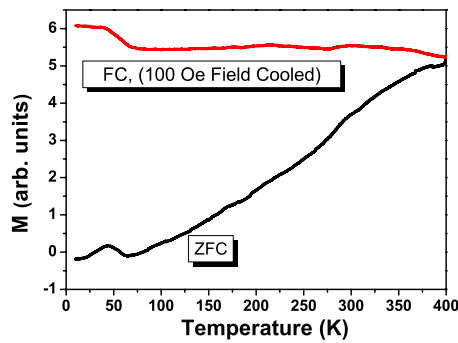
FIG. 5. (Color online) The temperature dependence of the magnetization of Co-implanted BaTiO$_3$ (fluency—1.0×10^{17} ion/cm^2) measured in FC and ZFC regimes.

Additionally, small peaks in the both ZFC and FC curves at low temperatures is attributed to the interfacials magnetic moments of the particles that are "frozen"[47,48] in a certain directions at temperatures lower than 40 K. The magnetic hysteresis loops at various temperatures measured between 50 and 400 K on applying the magnetic field with intensities up to ± 5 kOe are presented in Fig. 6. In all measurements the field is applied in the directions parallel to the implanted

surface of BaTiO$_3$. The recorded $M(H)$ loops confirm the ferromagnetic-like behavior. The coercive field decreases significantly with increasing the temperature and reaches to zero on approaching $T_b \sim 400$ K (Fig. 7). Thus, the results of the magnetization measurements also support the origin of observed ferromagnetic behavior in granular ferromagnetic layer formed in a result of Co implantation of BaTiO$_3$.

E. Magnetoelectric coupling

The main aim of this investigation is offering of new type of magnetoelectric composite structures on the base of ferroelectric perovskite crystals implanted by paramagnetic ions. In this point of view, the study of the influence of the electric field on magnetic properties as well as the study of the influence of the magnetic field on dielectric properties is of great interest.[2,49,50] The results of these studies could check the presence of magnetoelectric coupling in Co-implanted BaTiO$_3$ and show the promise of magnetic nanocomposites based on ion-implanted ferroelectric perovskites for potential magnetoelectric applications.

Figure 8 shows the results of FMR investigations of Co-implanted BaTiO$_3$ on applying the electric field on the sample. The measurements were performed in out-of-plane
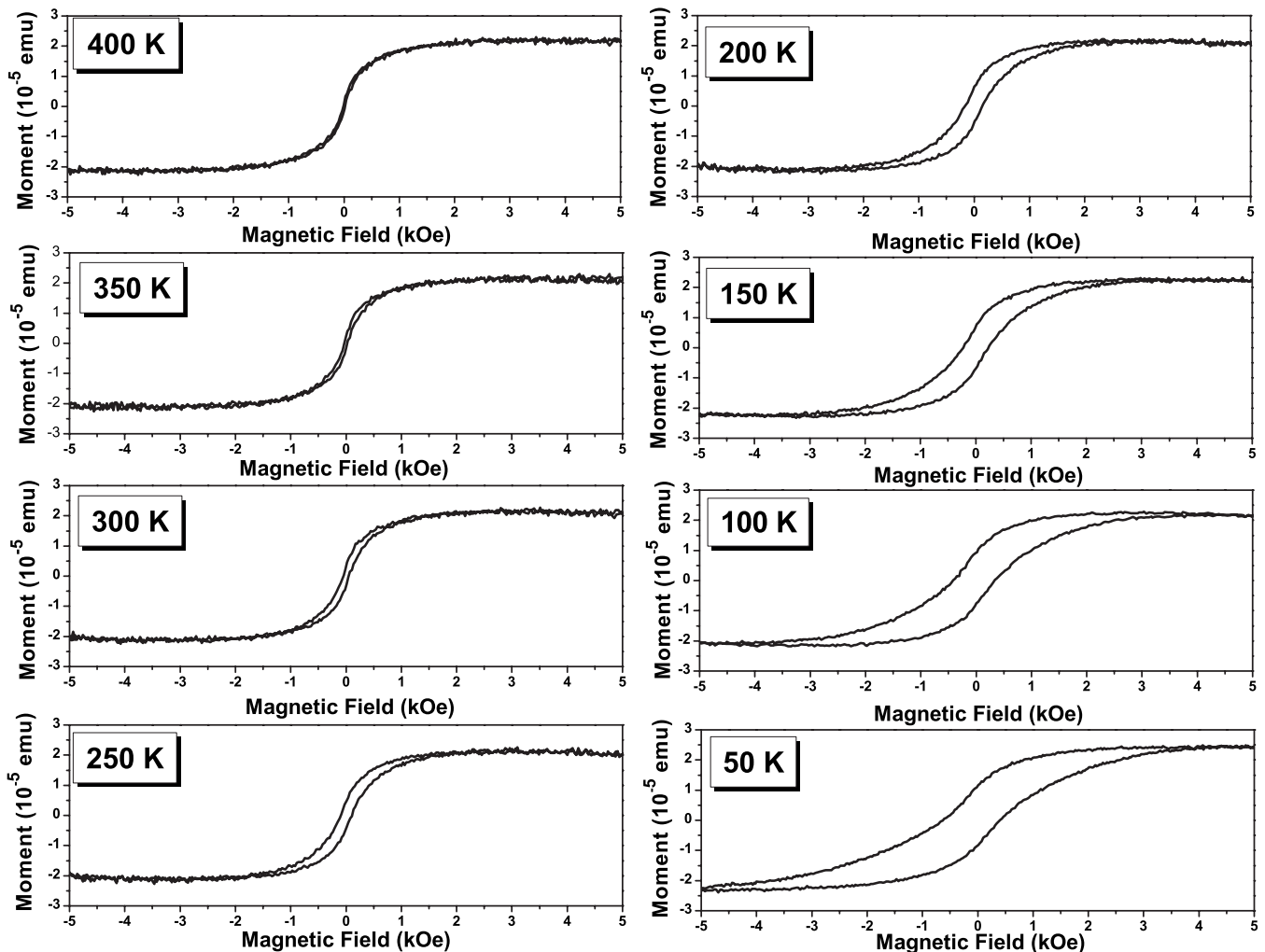
FIG. 6. Ferromagnetic hysteresis loops of Co-implanted BaTiO$_3$ (fluency—1.0×10^{17} ion/cm^2) measured at different temperatures.
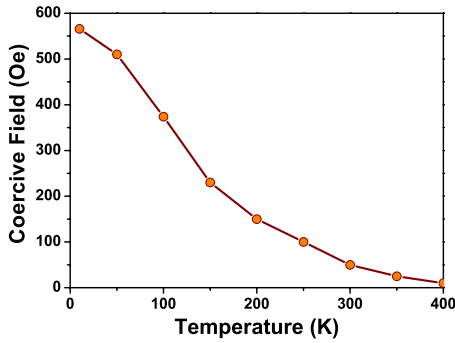
FIG. 7. (Color online) Temperature dependence of the coercive field of Co-implanted $BaTiO_3$ (fluency—1.0×10^{17} ion/cm^2).

geometry; both static electric and static magnetic fields were applied in the perpendicular direction to the implanted surface plane. So, taking into account the fact that the effective magnetization is observed to lie in the implanted surface plane, we observed transverse magnetoelectric effect, which includes the change in the value of effective magnetization in a result of increasing of electric field value applied in perpendicular direction. As it is seen in Fig. 8, the increasing of the intensity of the electric field up to 7.5 kV/cm brought to decreasing of the ferromagnetic resonance field value by amount 45 Oe.

Additionally, the study of the influence of applied magnetic field on dielectric properties of Co-implanted $BaTiO_3$ crystal revealed also very interesting result, which is presented in Fig. 9. The observed magnetocapacitance effect is another evidence of magnetoelectric coupling in Co:$BaTiO_3$ composite structure. It has been revealed that the capacitance of the samples exhibits considerable increase on increase in the applied magnetic field intensity. The relative changes in the capacitance are estimated to be about 5% on applying the magnetic field with intensity of 2 T at room temperature. This is a very remarkable value, comparing with the data on various magnetoelectric composites given in the literature.[51,52] Another interesting result is the magnetic field behavior of the capacitance, which possesses nonlinear character similar to magnetic field behavior of the magnetization

in ferromagnetic structures. This result can be interpreted as the evidence of magnetoelectric interaction between dielectric polarization and magnetization in Co:$BaTiO_3$ composite structure, which is also called as magnetodielectric effect.

The observed phenomenon can be explained on the base of well-known interpretation of strong magnetoelectric coupling in ferroelectric-ferromagnetic composite structures.[3] A strong ME effect could be realized in the composite consisting of magnetorestrictive and piezoelectric effects so that an efficient magnetomechanical-piezoelectric coupling between the two phases is achieved.[1,3] In this case the magnetoelectric effect originates from the elastic interaction between the magnetostrictive and piezoelectric subsystems. In a magnetic field, the magnetostriction in the magnetostrictive phase gives rise to mechanical stresses that are transferred into the piezoelectric phase, owing to the piezoelectric effect, resulting in an electric polarization of the ferroelectric-piezoelectric phase.

IV. CONCLUSIONS

The magnetic resonance and magnetization studies of Co-implanted $BaTiO_3$ perovskite crystal reveal the presence of anisotropic EMR spectra from Fe impurities in the substrate and ferromagnetic behavior due to Co nanoparticles. EMR spectra indicate that the $BaTiO_3$ substrates used in this study contain Fe^{3+} impurities located at Ti^{4+} tetragonal sites. The temperature-dependent EMR spectra shows the structural phase transition from the tetragonal to orthorhombic phase in Fe:$BaTiO_3$. The calculated ZFS parameters in different temperatures may help to extract the structural information from the changing of actual site symmetry of Fe^{3+} in ZFS Hamiltonian.

The results of SPM analysis of ZFS parameters for Fe^{3+} ions are discussed and compared with experimental EMR data. A good fit of EMR and FMR experimental data using the appropriate values with theoretical results is obtained. All results show good agreement between theory and experiment. Additionally, the analysis of low-temperature EMR measurements has been performed and ZFS parameters for

(a)

(b)
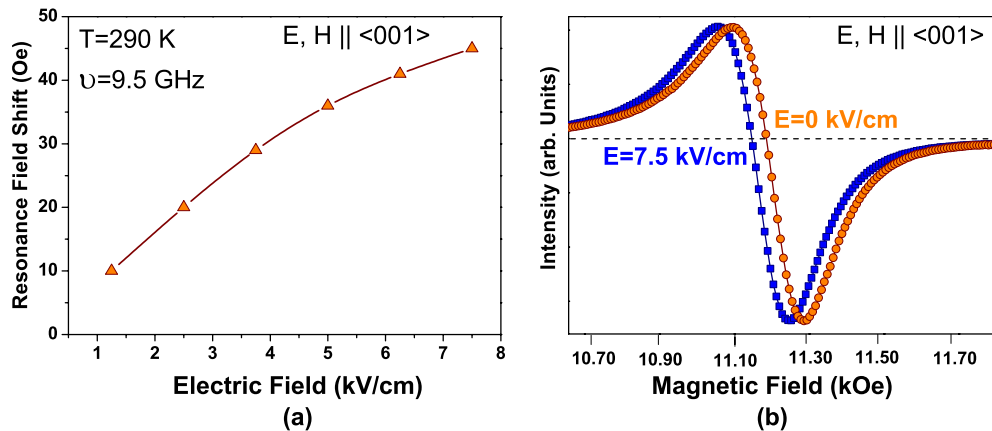
FIG. 8. (Color online) (a) The shift in the resonance field as a function of electric field. (b) Electric field dependence of FMR spectra obtained for perpendicular orientation of the static magnetic field with respect to implanted surface plane of Co-implanted $BaTiO_3$ (fluency—1.0×10^{17} ion/cm^2). The FMR spectrum shift to low-field region (down-shift) when E is increased from 0 to 7.5 kV/cm.
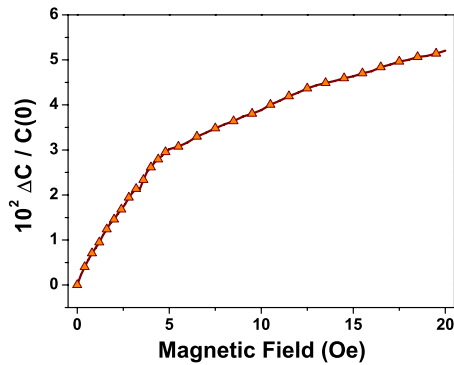
FIG. 9. (Color online) Relative change in the capacitance of Co-implanted $BaTiO_3$ as a function of external magnetic field.

Fe^{3+} ions in orthorhombic phases of $BaTiO_3$ have been obtained.

It has been revealed that the implantation of Co into single-crystal $BaTiO_3$ using different fluences of metal concentrations produces a ferromagnetic behavior which is due to the ferromagnetic granular film constructed on the surface of ferroelectric substrate. The magnetization and FMR spectra measured at different crystalline orientations of substrate with respect to the applied magnetic field show an out-of-plane uniaxial magnetic anisotropy in Co-implanted $BaTiO_3$. The observed phenomena are discussed on the base of strong magnetic dipolar interaction between Co nanoparticles due to decreasing of interparticle distance with increasing implantation dose. The magnetization measurements showed that the blocking temperature of superparamagnetic Co nanoparticles is about 400 K.

The investigations of magnetoelectric coupling have been performed. In this frame, the FMR spectra in out-of-plane orientation showed remarkable changes in resonance field value on increasing the intensity of perpendicularly applied electric field, which means the changing of effective magnetization of the granular magnetic layer on applying the electric field. On the other hand, considerable magnetocapacitance effect has been observed in Co-implanted $BaTiO_3$, which can be attributed to increase in ferroelectric polarization of $Co:BaTiO_3$ composite structure on applying the magnetic field. These results show the promise of magnetic nanocomposites based on Co-implanted ferroelectric perovskite $BaTiO_3$ crystal for potential magnetoelectric applications.

[1] W. Eerenstein, N. D. Mathur, and J. F. Scott, Nature (London) **442**, 759 (2006).

[2] M. Fiebig, J. Phys. D **38**, R123 (2005).

[3] C.-W. Nan, M. I. Bichurin, S. Dong, D. Viehland, and G. Srinivasan, J. Appl. Phys. **103**, 031101 (2008).

[4] G. Dearnaley, J. H. Freeman, R. S. Nelson, and J. Stephen, *Ion Implantation* (North-Holland, Amsterdam, 1973).

[5] C. Rudowicz and S. K. Misra, Appl. Spectrosc. Rev. **36**, 11 (2001).

[6] K. A. Müller, J. Phys. (Paris) **42**, 551 (1981).

[7] K. A. Müller and J. C. Fayet, in *Structural Phase Transitions Studied by Electron Paramagnetic Resonance*, edited by K. A. Müller and H. Thomas (Springer, Berlin, 1991), p. 1.

[8] E. Possenriede, P. Jacobs, and O. F. Schirmer, J. Phys.: Condens. Matter **4**, 4719 (1992).

[9] R. N. Schwartz and B. A. Wechsler, Phys. Rev. B **48**, 7057 (1993).

[10] C. Rudowicz and P. Budzynski, Phys. Rev. B **74**, 054415 (2006).

[11] H. G. Maguire and L. V. C. Rees, J. Phys. (Paris), Colloq. **33**, C2-173 (1972).

[12] C. Rudowicz, Magn. Reson. Rev. **13**, 1 (1987); **13**, 335 (1988).

[13] A. Abragam and B. Bleaney, *Electron Paramagnetic Resonance of Transition Ions* (Clarendon Press, Oxford, 1970).

[14] C. Rudowicz, J. Phys. C **18**, 1415 (1985); **18**, 3837 (1985).

[15] C. Rudowicz and C. Y. Chung, J. Phys.: Condens. Matter **16**, 5825 (2004).

[16] E. Siegel and K. A. Müller, Phys. Rev. B **19**, 109 (1979).

[17] D. J. Newman and E. Siegel, J. Phys. C **9**, 4285 (1976).

[18] M. Heming and G. Lehmann, in *Electron Magnetic Resonance of the Solid State*, edited by J. A. Weil (Canadian Society for Chemistry, Ottawa, 1987), p. 163.

[19] D. J. Newman and B. Ng, *Crystal Field Handbook* (Cambridge University Press, Cambridge, U.K., 2000).

[20] D. J. Newman and B. Ng, Rep. Prog. Phys. **52**, 699 (1989).

[21] D. J. Newman and B. Ng, J. Phys.: Condens. Matter **1**, 1613 (1989).

[22] D. J. Newman and W. Urban, Adv. Phys. **24**, 793 (1975).

[23] D. J. Newman, Adv. Phys. **20**, 197 (1971).

[24] C. Rudowicz, J. Phys. C **20**, 6033 (1987).

[25] D. L. Decker, K. Huang, and H. M. Nelson, Phys. Rev. B **66**, 174103 (2002).

[26] T. Sakudo, J. Phys. Soc. Jpn. **18**, 1626 (1963).

[27] T. Sakudo and H. Unoki, J. Phys. Soc. Jpn. **19**, 2109 (1964).

[28] M. B. Klein and R. N. Schwarz, J. Opt. Soc. Am. B **3**, 293 (1986).

[29] L. Rimai and G. A. deMars, Phys. Rev. **127**, 702 (1962).

[30] M. D. Sastry, M. Moghbel, P. Venkateswarlu, and A. Darwish, Pramana **56**, 667 (2001).

[31] M. Actis and F. Michel-Calendini, Int. J. Quantum Chem. **61**, 657 (1997).

[32] W. C. Zheng, Physica B **215**, 255 (1995).

[33] E. Siegel and K. A. Müller, Phys. Rev. B **20**, 3587 (1979).

[34] H. D. Megaw, Acta Crystallogr. **5**, 739 (1952).

[35] *Ferro- and Antiferroelectric Substances*, Landolt Börnstein New Series Group III, Vol. 3, edited by K. H. Hellwege and A. M. Hellwege (Springer-Verlag, Berlin, 1969), p. 51.

[36] M. Uludoğan and T. Çağın, Turk. J. Phys. **30**, 277 (2006).

[37] B. Ravel, E. A. Stern, R. I. Vedrinskii, and V. Kraizman, Ferroelectrics **206**, 407 (1998).

[38] W. Zhong, D. Vanderbilt, and K. M. Rabe, Phys. Rev. Lett. **73**, 1861 (1994).

[39] G. N. Kakazei, A. F. Kravets, N. A. Lesnik, M. M. Pereira de Azevedo, Yu. G. Pogorelov, and J. B. Sousa, J. Appl. Phys. **85**, 5654 (1999).

[40] S. Kazan, A. G. Şale, Ju. I. Gatiiatova, V. F. Valeev, R. I. Khaibullin, and F. A. Mikailzade, Solid State Commun. **150**, 219 (2010).

[41] C. Okay, B. Z. Rameev, R. I. Khaibullin, M. Okutan, F. Yildiz, V. N. Popok, and B. Aktas, Phys. Status Solidi A **203**, 1525 (2006).

[42] A. Butera, J. N. Zhou, and J. A. Barnard, Phys. Rev. B **60**, 12270 (1999).

[43] H. Suhl, Phys. Rev. **97**, 555 (1955).

[44] M. Belmeguenai, S. Mercone, C. Adamo, L. Méchin, C. Fur, P. Monod, P. Moch, and D. G. Schlom, Phys. Rev. B **81**, 054410 (2010).

[45] A. L. Stepanov, R. I. Khaibullin, B. Z. Rameev, A. Reinholdt, and U. Kreibig, Tech. Phys. Lett. **30**, 151 (2004).

[46] S. Tomita, K. Akamatsu, H. Shinkai, S. Ikeda, H. Nawafune, C. Mitsumata, T. Kashiwagi, and M. Hagiwara, Phys. Rev. B. **71**, 180414(R) (2005).

[47] J. L. Dormann, D. Fiorani, and E. Tronc, Adv. Chem. Phys. **98**, 293 (1997).

[48] D. Srikala, V. Singh, A. Banerjee, and B. Mehta, arXiv:1003.1855, J. Nanosci. Nanotechnol. (to be published).

[49] M. I. Bichurin, R. V. Petrov, and Yu. V. Kiliba, Ferroelectrics **204**, 311 (1997).

[50] G. Srinivasan and Y. K. Fetisov, Ferroelectrics **342**, 65 (2006).

[51] H. Zheng, J. Wang, S. E. Lofland, Z. Ma, L. Mohaddes-Ardabili, T. Zhao, L. Salamanca-Riba, S. R. Shinde, S. B. Ogale, F. Bai, D. Viehland, Y. Jia, D. G. Schlom, M. Wuttig, A. Roytburd, and R. Ramesh, Science **303**, 661 (2004).

[52] T. Kimura, S. Kawamoto, I. Yamada, M. Azuma, M. Takano, and Y. Tokura, Phys. Rev. B **67**, 180401(R) (2003).